Monthly Notices
of the
ROYAL ASTRONOMICAL SOCIETY

MNRAS **476,** 4794–4805 (2018)
Advance Access publication 2018 February 27

doi:10.1093/mnras/sty524

An algorithm for determining the rotation count of pulsars

Paulo C. C. Freire★ and Alessandro Ridolfi

Max-Planck-Institut für Radioastronomie, Auf dem Hügel 69, D-53121 Bonn, Germany

Accepted 2018 February 23. Received 2018 February 20; in original form 2018 January 11

ABSTRACT

We present here a simple, systematic method for determining the correct global rotation count of a radio pulsar; an essential step for the derivation of an accurate phase-coherent ephemeris. We then build on this method by developing a new algorithm for determining the global rotational count for pulsars with sparse timing data sets. This makes it possible to obtain phase-coherent ephemerides for pulsars for which this has been impossible until now. As an example, we do this for PSR J0024−7205aa, an extremely faint Millisecond pulsar (MSP) recently discovered in the globular cluster 47 Tucanae. This algorithm has the potential to significantly reduce the number of observations and the amount of telescope time needed to follow up on new pulsar discoveries.

Key words: methods: data analysis – pulsars: general – pulsars: individual: PSR J0024–7205aa.

1 INTRODUCTION

In the 50 yr since the discovery of radio pulsars, their study has been a major scientific success story. They are extremely versatile and powerful tools for studying fundamental physics, in particular the study of gravity, the fundamental properties of space–time and of gravitational waves (see Wex 2014; Berti et al. 2015 and the many references therein). Measurements of large neutron star masses (e.g. Antoniadis et al. 2013; Fonseca et al. 2016) had profound implications for the study of cold nuclear matter at supra-nuclear densities (see Özel & Freire 2016 and references therein), a fundamental question in nuclear physics. The orbital properties and abundance of double neutron star systems provided the first estimates of the rate of NS–NS mergers, the first 'guaranteed' source of events for ground-based gravitational wave detectors. Furthermore, pulsars can be used to detect very low frequency gravitational waves directly (The NANOGrav Collaboration 2015; Desvignes et al. 2016; Reardon et al. 2016; Verbiest et al. 2016).

Apart from these 'fundamental physics' applications, radio pulsars are also superb astrophysical tools: they allow a much deeper understanding of the late stages of the evolution of massive stars, including the supernova events (important for understanding the origin of the most useful pulsars, the recycled pulsars, see e.g. Lorimer 2008; Tauris et al. 2017), the dynamics and history of globular clusters and the ionized interstellar medium.

1.1 Pulsar timing

Most of these applications rely on a single, simple technique, *pulsar timing*. This technique achieves its full power for recycled pulsars. Put simply, this consists of the study of the times of arrival (TOAs) of the pulses (normally determined by adding many individual pulses coherently in phase) at one or several telescopes, most often radio telescopes. These TOAs can be determined very accurately, in some cases with precisions better than 100 ns, but more commonly a few μs; they correspond to times where a particular longitude of the pulsar (normally close to the spin phase where the observed radio emission is at a maximum) is aligned towards the Earth. Therefore, in between any two radio pulses the pulsar has rotated an integer number of times.

A good timing solution (henceforth a *phase-coherent ephemeris*) must be capable of accurately predicting the TOAs. This ephemeris consists of a specified mathematical description with a few crucial free parameters that describe the spin of the pulsar plus the transformation between the reference frame of the pulsar and that of the receiving telescope. In the reference frame of most recycled pulsars, their rotation can be described by a spin frequency (ν), plus a small, but constant and negative spin frequency derivative ($\dot{\nu}$). In the reference frame of the receiving radio telescope, these arrival times are affected by the motion of the pulsar relative to the radio telescope. This has several components: the observatory's motion caused by the Earth's rotation, the motion of the Earth relative to the Solar system barycentre (SSB), and the motion of the pulsar relative to the SSB, which might be affected by the pulsar's own orbital motion (if it happens to have any companion(s)). In order to correct for the movement of the radio telescope relative to the SSB, we need to have an estimate of the position of the pulsar in the sky; i.e. the right ascension (α), declination (δ) and, for measurements spanning many years, the proper motion in these two coordinates (μ_α, μ_δ). Finally, if the pulsar is in a binary system, then its orbital motion can be normally parametrized by five Keplerian parameters: in the Damour & Deruelle (1986) model (known as the DD model), for example, these parameters are the orbital period (P_b), the semi-major axis of the pulsar's orbit projected along the line of sight (x), the orbital eccentricity (e), the longitude of periastron (ω), and

★ E-mail: pfreire@mpifr-bonn.mpg.de

the time of passage through periastron (T_0). In some cases, a few additional 'post-Keplerian' parameters can be measured, these are caused by geometric (Kopeikin 1996) and relativistic (e.g. Damour & Taylor 1992) effects. In the case of 'black widow' or 'redback' pulsars, where there are Newtonian perturbations to the orbit, additional parameters might be necessary (e.g. Shaifullah et al. 2016). It is clear from the number of parameters (and their measurement precision) that these phase-coherent ephemerides provide a wealth of scientific information.

These ephemerides are derived from the TOAs using a timing program, like TEMPO,[1] TEMPO2 (Hobbs, Edwards & Manchester 2006; Edwards, Hobbs & Manchester 2006) or PINT;[2] in what follows we will be using TEMPO because it allows a very simple implementation of the methods to be described. For each TOA, TEMPO will first correct it using tables where the local time standard at the radio telescope is compared to a more stable time-scale, e.g. the universal coordinated time (UTC). Then, the position of the radio telescope relative to the SSB is calculated, first by using Earth rotation tables to calculate where the radio telescope is relative to the Earth's centre, then by using a Solar system ephemeris (like DE 421, Folkner, Williams & Boggs 2008 or DE 430, Folkner et al. 2014) to translate the latter to the SSB. This vector is then projected along the direction to the pulsar (derived from α, δ, μ_α, and μ_δ) to calculate the effect of the motion of the radio telescope relative to the SSB on the TOAs. Then, if the pulsar is in a binary, a binary model (like the aforementioned DD model) is used to subtract the time delays caused by the orbital motion. It is only after this stage that TEMPO calculates the *residuals*: these are the TOAs minus the prediction of the model *for the corresponding rotation of the pulsar*. The best-fitting timing parameters are determined by varying the timing parameters in a way that minimizes the sum of the squares of the residuals.

1.2 The problem

In the last paragraph, we have placed the emphasis on one fundamental point, which is rarely discussed in the literature: TEMPO can only determine a phase-coherent ephemeris if it is comparing a TOA with the model estimate for that pulse, not the one before or after. This can only be achieved *after* the correct rotation count between any two TOAs (a set of integers) has been established. This is what we call a *global rotation count*.

As we will see, when a new pulsar is discovered, the rotation count within a single observation is generally well known. However, the rotation count between successive observations is generally *not* known. As we will show, this issue is easy to solve for most pulsars, but it is hard to solve if there are no closely spaced detections of the pulsar, as in the case of scintillating pulsars, or pulsars in eclipsing systems. In the case of very faint pulsars, the timing precision might be too poor for the determination of the rotation count even for closely spaced observations.

The number of known faint pulsars has been growing significantly, but the time available at the major radio telescopes that can detect them remains unchanged, this implies automatically less time available to follow up each new pulsar. This can be partly compensated by more sensitivity and larger bandwidths, but also a more careful coordination of observations, and by dropping many pulsars that are scientifically less rewarding.

However, as we will see below, even if a pulsar is seen to have a high scientific value and its observation becomes a priority at a particular radio telescope, finding the correct rotation count might still be extremely difficult to achieve. Frequent eclipses or the effects of scintillation mean that even a dense set of observations does not necessarily translate into a dense set of detections with a minimal useful signal-to-noise ratio (S/N). Thus, in some cases, a phase-coherent ephemeris has not been obtained to date.

1.3 Structure of the paper

In Section 2, we present the observations and measurements of TOAs for a recently discovered pulsar, PSR J0024−7205aa (henceforth 47 Tuc aa); an example of a pulsar for which no phase-coherent ephemeris could be derived until now, despite the large number of observations available. The TOAs from this pulsar are then used to illustrate the concepts discussed in this paper, always using TEMPO as a practical tool for deriving results: we believe that the use of this specific program on a specific example is helpful for the illustration of the concepts presented in the paper. In Section 3, we present the concept of global rotation count in more detail and describe a simple, standard method for achieving it that can be applied to most pulsars; this assumes familiarity with the TEMPO timing package. This standard method can determine global rotation counts for most pulsars but it cannot achieve this for 47 Tuc aa owing to the extreme sparsity of its detections. In Section 4, we highlight a method for determining the global rotation count for such pulsars with a minimal number of TEMPO iterations, and present its implementation as a UNIX shell script. In Section 5, we use this method to determine the rotation count of 47 Tuc aa, presenting a previously unavailable phase-coherent ephemeris for this pulsar and discussing the significance of its parameters. Finally, in Section 6, we summarize our results and highlight some of the possibilities opened up by the method discussed here.

Throughout this work, we will assume basic familiarity with the concepts of pulsar signal analysis, in particular dedispersion, folding and the use of low-noise pulse profile templates to estimate TOAs; for a review see Lorimer & Kramer (2004). We will introduce some concepts as we go along, whenever this happens the new concept is presented in italic.

2 OBSERVATIONS AND DATA REDUCTION OF 47 TUC AA

The pulsar discussed in this work, 47 Tuc aa, is one of the 25 radio millisecond pulsars (MSPs) known in the globular cluster NGC 104, also known as 47 Tucanae (henceforth 47 Tuc). All these pulsars are detected in the same data (the telescope beam covers all their positions simultaneously), obtained during 519 observations of 47 Tuc carried out from 1997 until 2013 (i.e. a time span of 16 yr) with the 64-m Parkes radio telescope in New South Wales, Australia. These observations are part of a long-term project dedicated to these pulsars. The project's scientific motivation, setup of the observations, data taking (with the Analogue Filterbank, or AFB) and reduction and some of its results are described by Ridolfi et al. (2016), Freire et al. (2017), and their references.

47 Tuc aa was discovered in this data set by Pan et al. (2016). With a spin period of only 1.845 ms, it is the fastest-spinning pulsar known in 47 Tuc. It also has the highest dispersion measure (DM) for any known pulsar in the cluster, 24.941(7) pc cm^{-3}. The detections of this object are extremely rare: in the 519 observations of the data set, the pulsar was only detected (in the sense of yielding at least

[1] http://tempo.sourceforge.net/.
[2] https://github.com/nanograv/PINT.

one usable TOA) on 22 occasions; this represents a detection rate of 4.2 per cent, and an average of 1.38 detections per year. In most of these detections the S/N is smaller than 6. Given this extreme sparsity, no phase-coherent ephemeris could be derived by Pan et al. (2016).

The reason for the small number of detections is the small flux density of the pulsar combined with diffractive scintillation: like most pulsars in 47 Tuc, 47 Tuc aa has a flux density that is well below the telescope's sensitivity limit. Most of these pulsars are only detectable when scintillation amplifies their signal (see e.g. Camilo et al. 2000). 47 Tuc aa is so faint that only very rarely is the scintillation amplification large enough to make the pulsar detectable, even in observations lasting 8 h. This means that although we can choose when to observe the cluster and the pulsars in it, we cannot choose when to detect any particular pulsar. This is also one of the reasons why, despite the lack of improvement of the sensitivity, new pulsars are still being discovered in this data set: for instance, 47 Tuc aa is not detected on the vast majority ($\sim$96 per cent) of observations, and other even fainter pulsars might be appearing even more infrequently.

Although no phase-coherent ephemeris was presented for 47 Tuc aa in Pan et al. (2016), the few detections of this object show that, after correction for the Doppler shift due to the Earth's motion, its spin period does not change measurably with time. This implies that, unlike most MSPs in 47 Tuc, this particular object is not part of a binary system. Apart from this, not much was known about it, in particular its location relative to the centre of the cluster, its proper motion or its spin period derivative. These parameters are exquisitely well determined for the other 22 MSPs in 47 Tuc with phase-coherent ephemerides (Ridolfi et al. 2016; Freire et al. 2017).

3 ROTATION COUNT AND HOW TO DETERMINE IT

3.1 Rotation count within an observation

In Fig. 1, we display one of the best detections of 47 Tuc aa, from an observation on modified Julian date (MJD) = 54314 (2007 August 2). In this plot, we can see that the pulsations appear at a constant spin phase. This shows conclusively that the estimate of the spin frequency ($\nu =$ 541.893 656 Hz), determined from the search procedure (Pan et al. 2016), is precise enough to predict the arrival times of the pulses within that observation. If the spin period were in error, we should see a drift of the pulse phase with time.

This can be confirmed with TEMPO in the following way:

(i) Group the 60 sub-integrations displayed in Fig. 1 into, for example, six longer sub-integrations and, using the techniques described in Ridolfi et al. (2016), make a single TOA for each sub-integration. A TOA list suitable for use in TEMPO looks like this:[3]

```
MODE 1
7 1390.000 54314.7954878129250 16.660 0.00000
7 1390.000 54314.8211805391308 17.735 0.00000
7 1390.000 54314.8468749751720 15.921 0.00000
7 1390.000 54314.8725694346731 21.125 0.00000
7 1390.000 54314.8982638745009 19.083 0.00000
7 1390.000 54314.9222205617143 19.950 0.00000
```

'MODE 1' flag indicates that TEMPO will make a weighted fit, with the weight of each TOA given by the inverse of its uncertainty. The first column indicates the radio telescope where the data were taken (in this case 7 identifies Parkes), the second column the central radio frequency in MHz, the third column is the TOA itself in MJD, the fourth column is the TOA uncertainty in μs and the last one indicates any previous DM corrections (none in this case).

(ii) Make a simple ephemeris file '47Tucaa.par' containing the best estimate of the spin frequency (we start from the estimate in Pan et al. 2016), no spin period derivative (this is generally very small), and the coordinates of the centre of 47 Tuc (the pulsar is not likely to be more than 1.2 arcmin away from that centre, see Freire et al. 2017, except for pulsar 47 Tuc X, see Ridolfi et al. 2016) and the proper motion of the cluster (Freire et al. 2017). We also put in a parallax derived from the known cluster distance (4.69 kpc,

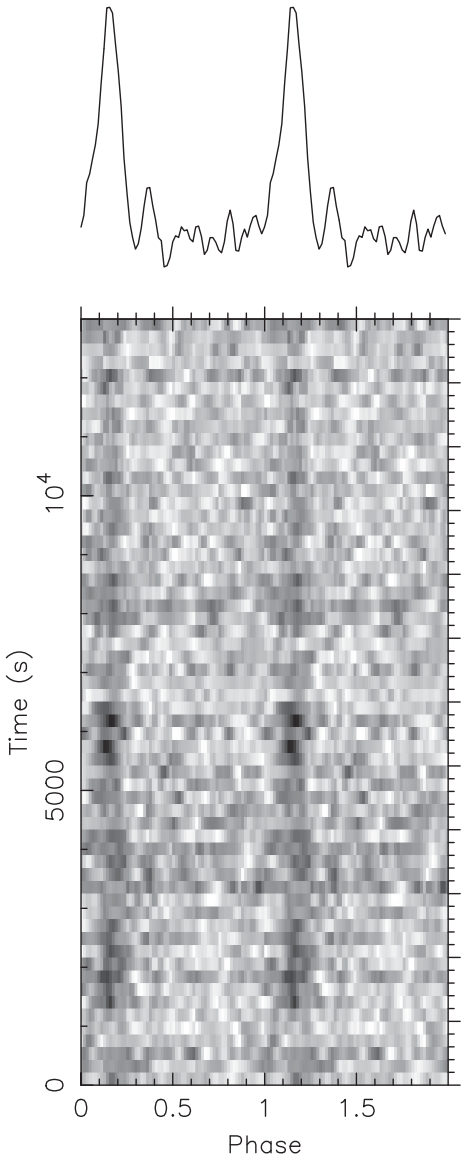

Figure 1. Best detection of 47 Tuc aa from an observation made on 2007 August 2. In the main grey-scale plot, we display the radio intensity at 20 cm (darker meaning larger intensity) as a function of the spin phase (displayed twice for clarity) and time, which is divided into 60 segments. As we can see the pulsar signal (the vertical grey line) does not drift perceptibly in phase, indicating that the spin period used to fold these data is accurate. The top plot represents the integrated radio intensity (vertical axis) as a function of spin phase, also displayed twice for clarity.

[3] The program accepts a variety of formats. In this case we chose use the 'Princeton' format because of its simplicity.

see discussion in Freire et al. 2017 and references therein); this has little effect on the timing but it is a known quantity anyway. This ephemeris looks like this:

```
PSR                J0024-7205AA
RAJ              00:24:05.67
DECJ             -72:04:52.62
PMRA                5.16
PMDEC              -2.85
PX                  0.2132
F0                541.893656 1
F1                  0
PEPOCH             51600
DM                 24.971
EPHEM               DE421
CLK               UTC(NIST)
UNITS               TDB
NITS 1
```

The flag '1' after F0 (the spin frequency, ν) means that we are fitting for this quantity. The reference epoch (given by the 'PEPOCH' flag) should generally be the barycentric time at which ν was measured. For a MSP with a small variation of the spin period, this is not so crucial, so we set PEPOCH to MJD = 51600 (2000 February 26) because it is the reference epoch used for all other ephemerides in Freire et al. (2017).

With these files, we then run TEMPO and look at the residuals. The pre-fit and post-fit residuals plots are displayed in Fig. 2; they have a reduced χ^2 of 4.24 and 1.06, respectively.

In that figure, TEMPO confirms what was already obvious from Fig. 1: the ephemeris '47Tucaa.par' predicts the correct rotation count within the observation: all TOAs are arriving within a very small phase window (from 0.0, defined automatically as the phase of the first TOA, to 0.03, a range that is of the same order as the TOA uncertainties). This means that the rotation count (5933 580) between the first and last TOAs estimated by our original ephemeris is correct, i.e. this group of TOAs is *phase-connected* (henceforth *connected*). After fitting for ν, the situation improves further, with all residuals even closer to 0.

From this set of TOAs, we can already have a very precise measurement of the spin frequency (or period, $P \equiv 1/\nu$). According to the TEMPO output (printed in file 'tempo.lis') the time elapsed between the first and last TOA is 3.04 h, more precisely $\delta T_{\rm t} = 10\,949.709\,495(26)$ s in the telescope reference frame and $\delta T_{\rm b} = 10\,949.713\,006(26)$ s in the SSB. Dividing the latter by the rotation count mentioned above, we obtain a barycentric spin period (P) of 0.001 845 380 5301 s, exactly the value returned by TEMPO. The uncertainty of the spin period δP should be the uncertainty of $\delta T_{\rm b}$ (26 μs) divided by the number of rotations, i.e. $\delta P = 4.8 \times 10^{-12}$ s. The uncertainty estimated by TEMPO is actually smaller (3.7×10^{-12} s) since it does not only take into account the first and last TOAs, but the other four intermediate ones as well. The parameters from this fit are presented in row 1 of Table 1.

For the remainder of this paper it is important to notice that the absolute phase of the pulses is immaterial, since TEMPO automatically assigns a spin phase of zero to the first TOA. All that matters is the rotation count between TOAs. By minimizing the residual rms, all that TEMPO did was to adjust the spin frequency in order to remove the *residual slope* from this single observation. Such residual slopes are essential because they give us the initial constraints on the global rotation count and the ephemeris to be derived from it.

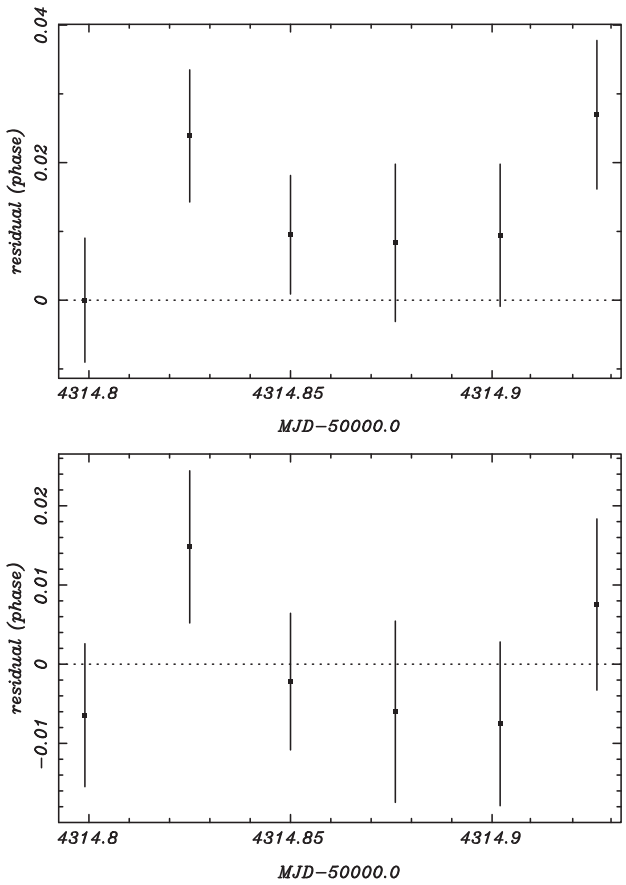

Figure 2. Pre-fit (top) and post-fit (bottom) residuals for the six TOAs derived from the best observation of 47 Tuc aa, taken on 2007 August 2. The horizontal axis represents time and the vertical axis represents the residual, in spin phase units. 0.01 of the spin phase corresponds to 18.5 μs, which is comparable to the TOA uncertainties.

3.2 Rotation count between observations

Although the rotation count within an observation is, as we have seen, generally well known, this is not the case for the rotation count between more widely spaced TOAs.

We can see this by repeating the procedure in the previous section for all available observations:

(i) Make TOAs for all observations where the pulsar has appeared. Whenever possible, make at least three TOAs – this is important for obtaining residual slopes from each day's data.
(ii) Use the same ephemeris as in the previous step.
(iii) Run TEMPO and look at the residuals.

For the ephemeris listed above, the pre-fit residuals are displayed in Fig. 3. These are scattered evenly through the whole spin phase, from −0.5 to 0.5, with no discernible pattern. This means that our first ephemeris is not precise enough to predict the rotation count between all these TOAs, otherwise all the residuals would be confined to a narrow range of phases, as in Fig. 2. Thus, the starting ephemeris is a *partial* ephemeris: it is certainly not phase-coherent.

This lack of precision stems from a variety of factors: (a) Lack of precision of the spin frequency ν (this is precise enough to predict TOAs for a few hours, but probably not enough to do so for many years), (b) the possibility that the sky position of the pulsar is slightly different from the position of the centre of 47 Tuc; this introduces small delays due to the Earth's motion that are none the less larger

Table 1. Post-fit parameters for several iterations described in the text. [a]Parameter not being fit, derived from initial assumptions (see the text).

Iteration number	ν (Hz)	$\dot{\nu}$ (10^{-15} Hz s^{-1})	α (hh:mm:ss.s)	δ (°: ′: ″)	Parameters fitted	TOAs fitted
1	541.893 6548(11)	0[a]	00:24 05.67[a]	−72:04:52.62[a]	ν	1 group
2	541.893 655 29(39)	0[a]	00:24:05.67[a]	−72:04:52.62[a]	ν	Initial groups + JUMPS
3	541.893 656 51(5)	0[a]	00:24:07.1(8)	−72:05:17.0(36)	ν, α, δ	Initial groups + JUMPS
4	541.893 6564(6)	12(6)	00:24:07.0(8)	−72:05:19.9(39)	$\nu, \alpha, \delta, \dot{\nu}$	Initial groups + JUMPS
5	541.893 6568(6)	4(4)	00:24:07.4(8)	−72:05:18.6(35)	$\nu, \alpha, \delta, \dot{\nu}$	1-d groups + JUMPS
6	541.893 654 948 99(18)	13.475(4)	00:24:07.2783(10)	−72:05:19.521(4)	$\nu, \alpha, \delta, \dot{\nu}, \mu_\alpha, \mu_\delta$	All connected

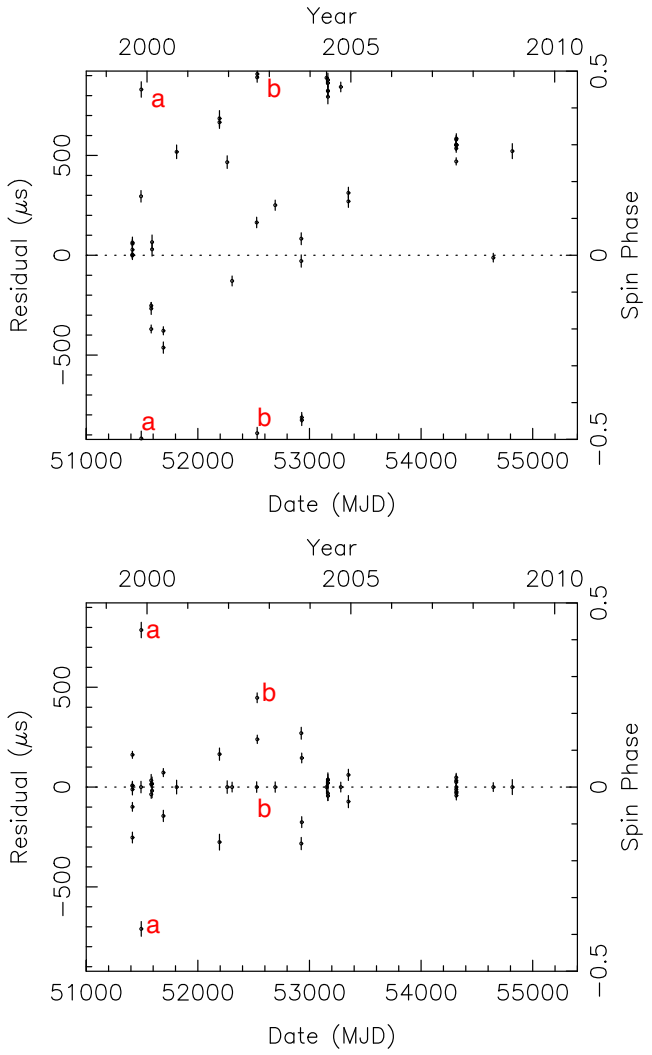

Figure 3. Pre-fit (top) and post-fit (bottom) residuals for all TOAs for 47 Tuc aa as a function of epoch. The pre-fit residuals are scattered evenly across the full spin phase space (between −0.5 and 0.5), i.e. our starting ephemeris is not precise enough to predict the phase even approximately. However, for TOAs derived from a single observation (i.e. those where we know there is connection), the residuals appear in nearly horizontal groups, this means that the predicted spin period for each observation is accurate. If a group of residuals appears near phase 0.5, then some residuals in that group might wrap around and appear near phase −0.5. So both TOAs indicated with 'a' and both indicated with 'b' really appear very close to each other in phase. Because of the mis-identification of the rotation number, the post-fit reduced χ^2 is 114.9.

than one rotation of the pulsar, and (c) the unknown variation of ν with time. In what follows, we will assume at first that this can be described by a single spin frequency derivative, $\dot{\nu}$.

In both plots of Fig. 3, we see that whenever multiple TOAs are derived from successive sub-integrations within the same observation, their residuals appear in (nearly) horizontal groups, except for two cases that appear near phase 0.5 that will be discussed below. This means that those groups of TOAs are connected (see Section 3.1). The time interval between two such groups is a *gap*; thus by definition the rotation count within a gap is not necessarily known at this stage.

3.3 Moving forward: a better ephemeris

The first step towards the determination of the rotation count is to make a more precise estimate of the spin frequency and other parameters using *all* connected TOA groups, right from the start. This has the great advantage that, for every step of the work, the estimates of all timing parameters are constrained by the residuals slopes from all connected TOA groups.

Since the initial ephemeris does not provide a reliable rotation count across all gaps, we cannot assume to know it. We can remove this assumption in TEMPO by fitting an arbitrary time offset for each group of connected TOAs. This can be achieved – in TEMPO – by bracketing the TOAs from all observations but one (in this case the last) with JUMP statements, as exemplified here:

```
MODE 1

JUMP
7 1390.000 51413.6357638815603 18.173 0.00000
7 1390.000 51413.6499999905185 23.038 0.00000
JUMP

JUMP
7 1390.000 51413.6895833852018 14.824 0.00000
7 1390.000 51413.7381944448891 14.797 0.00000
7 1390.000 51413.7868055551721 18.587 0.00000
7 1390.000 51413.8354166713418 22.973 0.00000
JUMP

JUMP
7 1390.000 51490.5017355131067 24.352 0.00000
JUMP

...
(some TOAs not shown here)
...
C DON'T BRACKET WITH JUMPS
7 1390.000 54816.49756962981 74 31.740 0.00000
```

Then, as before, run TEMPO. The pre-fit residuals are the same as displayed in the top of Fig 3.

Running TEMPO at this stage, we obtain the residuals displayed at the bottom of Fig. 3. These have a very high reduced χ^2 of 225.15. The reason for this (and this is something we should always beware during this process) is that there are groups of residuals close to the spin phase of 0.5: individual residuals in such groups might appear at spin phases near 0.5 *and* −0.5. This is happening for the two pairs of TOAs called 'a' (at MJD = 51492) and 'b' (at MJD = 52531), respectively. In this situation, the wrong rotation count is being assumed within those observations, so TEMPO cannot produce a good estimate of the parameters. In order to correct this, one should introduce or subtract (whichever is suitable) an extra rotation in between the TOAs in each group, so that they appear with the same phase in the pre-fit residual plot. This can be done with a PHASE +1/−1 statement in the TOA list, for the cases mentioned below these are

```
(...)
JUMP

7 1390.000 51492.5850727545785 31.229 0.00000
PHASE -1
7 1390.000 51492.6440955080127 32.860 0.00000
JUMP

C Optional
PHASE +1
(...)
  and
(...)
JUMP

7 1390.000 52531.6708365991755 24.719 0.00000
PHASE -1
7 1390.000 52531.7347222220090 20.900 0.00000
7 1390.000 52531.7968733372661 17.472 0.00000
JUMP

C Optional
PHASE +1
(...)
```

The optional PHASE +1 statements were introduced in both cases so that all residual phases continued being displayed in the interval from −0.5 to 0.5. Only after this correction, i.e. only after finding the correct rotation count within those observations, can TEMPO converge on an ephemeris with a reduced χ^2 close to 1. The pre and post-fit residuals as a function of epoch obtained after this correction are presented in Fig. 4.

In the lower plot of Fig. 4, all post-fit residuals appear within a narrow window of spin phases. This is mostly (but not entirely) a consequence of the fact that we have fitted time offsets for each group of connected TOAs. Solely removing these offsets does not eliminate the residual slopes for each group of connected TOAs; this is done by fitting the timing parameters.

Let us now exemplify this. If we fit only for ν, we obtain the spin frequency (presented in the second row in Table 1) that is more than twice as precise as the spin period estimate obtained from the best observation in Section 3.1. However, this ephemeris produced residuals with a reduced χ^2 of 3.79 – still with non-zero residual slopes within each day – so we might need to fit for (an)other parameter(s).

Because the total time span is larger than one year, it is possible to fit for ν, α, and δ, as the covariance between these parameters can be broken. If we do so, we obtain residuals with a reduced χ^2 of

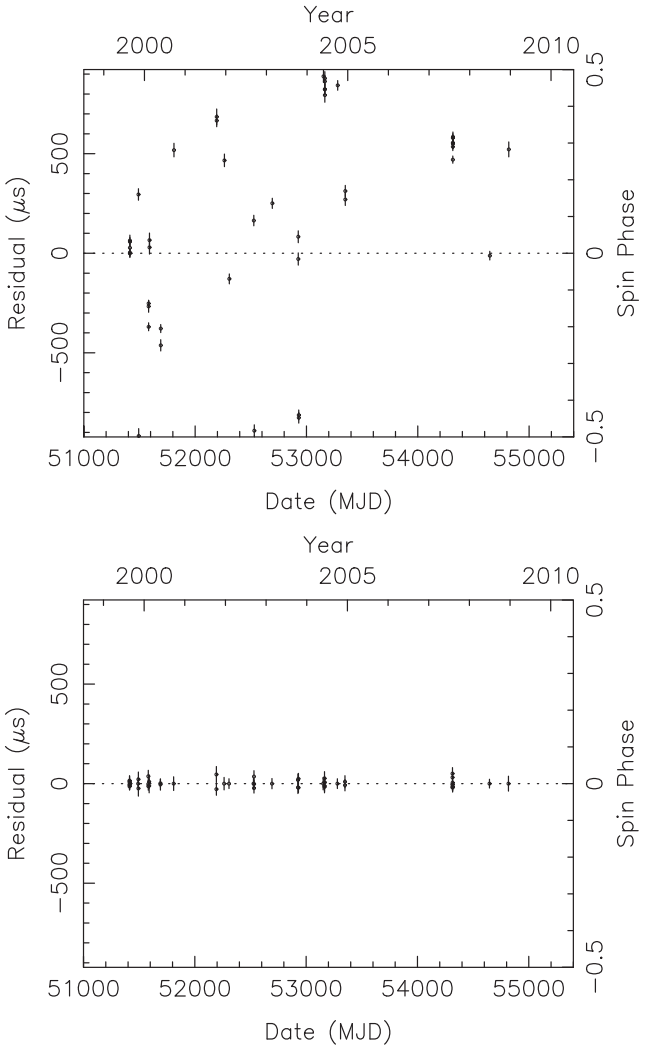

Figure 4. Pre-fit and post-fit residuals for all TOAs for 47 Tuc aa as a function of epoch, now with the correct rotation count for epochs 'a' and 'b'. Although the pre-fit residuals are scattered evenly across the full spin phase space (between −0.5 and 0.5), the post-fit residuals all appear near phase zero, with a reduced χ^2 near 1.9. This is partially a consequence of the fact that we are fitting an arbitrary time offset to each observation. Flattening the residuals slopes within individual observations constrains the timing parameters.

1.54, which is a major improvement. The solution we obtain then is presented in the third row of Table 1. We can see here that, although the spin frequency is not quite as precise as in the previous column, we can already pinpoint the location of the pulsar with a precision of a few arcseconds, which is a major improvement over the previous (and, as we can now see correct) assumption that the pulsar is near the centre of 47 Tuc.

If we fit for ν, α, and δ *and* $\dot{\nu}$, then the reduced χ^2 decreases to 1.40. The resulting best ephemeris is presented in the fourth row of Table 1. Although the resultant $\dot{P} \equiv -\dot{\nu}/\nu^2$ is not very significant, $(-4.0 \pm 2.0) \times 10^{-20}\,\mathrm{s\,s^{-1}}$, it is well within the range of what one finds for other pulsars in 47 Tuc. This implies that this parameter should be fit at this stage. Our starting ephemeris file is then the same as in Section 3.1, only with a few extra fitting flags (1's) added after α, δ, and $\dot{\nu}$ lines.

To summarize: although we have not determined the rotation count for a single gap, by using the JUMP statements we can use the

information contained in the residual slopes within all connected TOA groups to derive a reasonably precise position, period, and even a strong constraint on $\dot{\nu}$. These estimates cannot be derived from any individual group of TOAs.

3.4 Connecting the gaps

We now arrive at the most important step on the path to get the correct global rotation count for the pulsar. We look at the TOA list and find closely spaced groups of connected TOAs, i.e. short gaps. As an example, for the best detection of 47 Tuc aa, there is an observation earlier that day where the pulsar was also detected. Here, are the TOAs:

```
(...)

JUMP
7 1390.000 54314.7031249750801 15.335 0.00000
7 1390.000 54314.7515008653730 25.434 0.00000
JUMP

JUMP
7 1390.000 54314.7954878129250 16.660 0.00000
7 1390.000 54314.8211805391308 17.735 0.00000
7 1390.000 54314.8468749751720 15.921 0.00000
7 1390.000 54314.8725694346731 21.125 0.00000
7 1390.000 54314.8982638745009 19.083 0.00000
7 1390.000 54314.9222205617143 19.950 0.00000
JUMP

(...)
```

The question is now: is our original ephemeris (presented in Section 3.1) precise enough to predict the rotation count for this gap or not?

To find out, we comment out the inner pair of JUMP statements and introduce a PHASE +N statement, where N is an integer that determines the correction to the rotation count predicted by the ephemeris. In what follows, such integers (or combinations of k integers when discussing k gaps) are referred to as *k-gap solutions*, a 1-gap solution will be referred to simply as a *solution*.

```
(...)

JUMP
7 1390.000 54314.7031249750801 15.335 0.00000
7 1390.000 54314.7515008653730 25.434 0.00000
C JUMP
PHASE +0
C JUMP
7 1390.000 54314.7954878129250 16.660 0.00000
7 1390.000 54314.8211805391308 17.735 0.00000
7 1390.000 54314.8468749751720 15.921 0.00000
7 1390.000 54314.8725694346731 21.125 0.00000
7 1390.000 54314.8982638745009 19.083 0.00000
7 1390.000 54314.9222205617143 19.950 0.00000
JUMP

(...)
```

Now we run TEMPO, still with the original ephemeris. Assigning the integers -3, -2, -1, 0, 1, 2, and 3 to N, we obtain the following values for the reduced χ^2: 2063.0, 914.1, 226.9, 1.37, 237.5, 935.3, and 2094.8 (see Fig. 5).

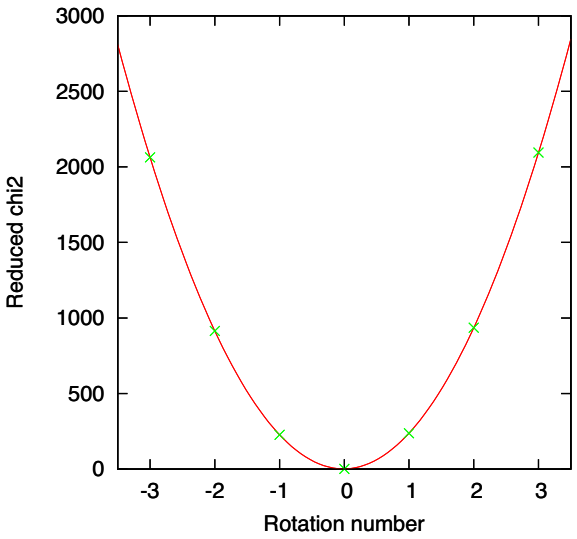

Figure 5. Reduced χ^2 as a function of the solution for the small gap in MJD = 54314. The values derived by TEMPO (green crosses) follow closely a parabolic curve; the latter is represented by the solid red line.

The quality of the fit is much higher for $N = 0$ (with a reduced χ^2 of 1.37) than for the second best fit (-1, where the reduced $\chi^2 = 226.9$). In such cases we can say with great confidence that there is a unique *acceptable solution*, '0'. This means that the rotation count of this gap is *unambiguous*, and in this case identical to the rotation count predicted by the initial ephemeris.

In this situation we can eliminate the gap, i.e. declare the groups on both sides to be mutually connected (in what follows, we simply describe this as *connecting the gap*). Because the gap has been connected, there is no need to reintroduce its JUMP statements in TOA list, but whatever PHASE +N statement worked best should stay. This connection results in more tightly constrained timing parameters.

In Fig. 5, we can see that the relation between the reduced χ^2 and N follows very closely a parabola, which is depicted by the solid red line. In the sections that follow, we make use of this fact.

3.5 Connecting the remaining gaps

After this stage, we look for other gaps shorter than 1 d. The two gaps we found (within MJD 51413 and 53164) also have unique solutions, in both cases 0, so both gaps can be connected. Since we now have slightly larger connected TOA groups, the post-fit timing parameters will be more precise. However, as we can see in the fifth row of Table 1, the improvement in this case is marginal.

In order to proceed, we must try to find other gaps with unique solutions, since such gaps can be immediately connected. The longer connected data set will then result in an ephemeris with more tightly constrained parameters; the latter will more likely make other gaps unambiguous. This is a runaway process, which means that, using this technique, we can, for most pulsars, determine unique solutions for all gaps, i.e. determine their global rotation count. This can be done even if the detections appear to be very sparse at first – all that matters is that there is a good distribution of *gap lengths*.

We will mention here a technical detail of this process, which will become apparent to anyone using this technique. Although the solutions for the shorter gaps will be relatively small integers, as the length of the gaps increases, the magnitude of the solutions

increases significantly. In order to mitigate the problem, the initial ephemeris can be replaced with the post-fit ephemeris calculated by TEMPO at any stage. For instance, we could have replaced the initial guess ephemeris in Section 3.1 with the better ephemeris derived in the previous section. For this to work, all previous PHASE +N statements in the TOA list must be commented out, since the corresponding rotation count is already taken into account by the new starting ephemeris. After such a change, however, we must always be careful about groups of TOAs at phases close to 0.5, as mentioned in Section 3.3.

Another important point to keep in mind is that for this technique to succeed, three conditions must be met:

(a) The TOAs must be accurate. If one TOA is for some reason in error, it will derail the whole process. For this reason, we must be careful with the selection of the pulse profiles while deriving TOAs.

(b) The TOAs should be consistent with each other (i.e. preferably come from the same telescope and timing instrument), also the template used to derive them should be the same.

(c) The pre-fit ephemeris must contain an appropriate set of timing parameters. For many isolated pulsars, α, δ, ν, and $\dot{\nu}$ are perfectly adequate; as we will see this is also the case for 47 Tuc aa. For longer time-scales, proper motion parameters might be necessary. However, even among isolated pulsars, particularly the younger ones, there are phenomena like glitches and timing noise that can greatly complicate the analysis.

When sparsely detected pulsars are part of binary systems (something that becomes immediately apparent from the variation of the spin period), we can make a preliminary determination of the orbital parameters from the observed spin periods and their derivatives using the method presented by Freire, Kramer & Lyne (2001a);[4] this was used to find the orbits of several pulsars in 47 Tuc. Those initial orbital parameters can then be refined by fitting the observed Doppler-shifted spin period as a function of time to a Keplerian model (something that can be done using a program like FITORBIT).

Phase-coherent ephemerides for such pulsars can be derived using the method we have just described above; however, to achieve that we must exercise good judgment on the binary parameters that must be fit. For a pulsar in wide, nearly circular orbit with a compact object, it is likely that fitting for Keplerian parameters from the start will be enough to find phase connection. If the orbit is compact and eccentric, then fitting for the rate of advance of periastron ($\dot{\omega}$) from the start might be necessary. In the case of eclipsing binary pulsars, then unpredictable changes in the orbital period must also be taken into account.

Back to 47 Tuc aa, and before we continue, we note that at this stage of the work the reduced χ^2 of the residuals is 1.40. Our previous experience timing other faint MSPs suggests this is likely to be caused by a slight underestimate of the TOA uncertainties. We can fix this by re-scaling the latter. In TEMPO, this is done by introducing a flag in the TOA list called EFAC, followed by a numerical value. All TOA uncertainties are then multiplied by this factor. In what follows, we use an EFAC of $\sqrt{\chi^2_{\rm red}} \simeq 1.185$. In this way, the reduced χ^2 becomes 1.0. This (slightly) increases the uncertainties of the timing parameters to more realistic values.

[4] The related CIRCORBIT software can be found at http://www3.mpifr-bonn.mpg.de/staff/pfreire/programs/circorbit.tar.

4 SIEVING SOLUTIONS

Apart from the single-day gaps mentioned in Section 3.5, there are, in the case of 47 Tuc aa, no wider gaps with unique solutions, i.e. all remaining gaps are *ambiguous*. In such cases it is not clear how to proceed.

In what follows, we will address this problem. We start by presenting an automatic method for finding and listing all acceptable solutions for each gap, this is called the *gap mapper*. By acceptable solutions we mean a solution having a reduced $\chi^2 < 2.0$, where that factor should not be too large as to allow an exceedingly large number of solutions, but it should not be so small as to exclude the correct solution, which might have a reduced χ^2 larger than 1.0. As we will see in Section 5.1, the eventual correct global solution has, using the four parameters being fit, a reduced $\chi^2 = 1.39$ (already using the EFAC factor of 1.185 mentioned above). Using a smaller χ^2 threshold might have excluded the correct solution. The limit of 2.0 is chosen because for most MSPs the reduced χ^2 in their published timing solutions is smaller than that.

4.1 Mapping a gap

One tool we will need to do the connection is to learn how to find the best solutions for any gap automatically. An efficient method to achieve this can be derived from Fig. 5 in Section 3.5: the reduced χ^2 varies as a parabola. We can find the minimum of a parabola if we sample it (i.e. use TEMPO to evaluate the reduced χ^2) for three (not necessarily acceptable) solutions. We generally choose these to be $-b$, 0, and b, with $b = 5$ being a good choice. In this case, then the minimum will be the integer M closest to

$$m = \frac{b}{2}\frac{\chi^2(-b) - \chi^2(b)}{\chi^2(b) + \chi^2(-b) - 2\chi^2(0)}. \quad (1)$$

Then, starting from M, we evaluate the integers immediately above and below it to establish the quality of fits, keeping a record of the acceptable solutions.

Using this simple device, we have mapped all the gaps in our 47 Tuc aa data set. For each gap i we list in Table 2 the best solution (M_i) and the number of acceptable 1-gap solutions (n_i) around it (roughly one half of that number of solutions above and below M_i).

4.2 Sieving

One possible way of finding the timing solution for 47 Tuc aa would be to try all possible combinations of acceptable solutions for the 21 gaps. However, this would clearly be impractical: the product of all n_i for this data set is

6 894 108 365 755 450 688 986 274 510 929 920 000,

or approximately 6.9×10^{36}. While mapping these gaps each TEMPO iteration took about 0.17 s; this means that, with the same computer, the whole process would take 3.7×10^{28} yr. As we will see below, the vast majority of these calculations are unnecessary.

We now describe the fundamental concept of the solution-finding algorithm. Although in the previous step we are not able to find a single unambiguous gap, we can assume, for one of the gaps (say, number 2), that one of its two acceptable 1-gap solutions (-1 and 0) is in turn correct. For each of these assumptions we try to find (using the gap mapper described in the previous section) acceptable solutions for a second gap, let's say number 11 (this gap should be chosen in order to yield the smallest possible number of acceptable solutions, i.e. it should be a short gap). If we find such a solution,

Table 2. Unconnected gaps in the 47 Tuc aa TOA data set and corresponding best solution for each gap (M_i) and number of acceptable solutions (n_i).

i	Gap	M_i	n_i
1	51413–51490	−14	58
2	51490–51492	0	2
3	51492–51582	−53	86
4	51582–51589	−3	7
5	51589–51690	+8	115
6	51690–51809	+34	84
7	51809–52193	−38	192
8	52193–52262	−38	72
9	52262–52307	−27	46
10	52307–52526	+33	168
11	52526–52531	0	3
12	52531–52693	−81	146
13	52693–52925	+33	140
14	52925–52930	−1	5
15	52930–53152	−70	172
16	53152–53164	+5	13
17	53164–53280	+22	49
18	53280–53348	−36	80
19	53348–54314	−128	697
20	54314–54646	−74	304
21	54646–54816	−37	168

then together with the solution for gap 2 being assumed this makes a new 2-gap solution. Then, assuming each 2-gap solution we proceed to search for acceptable solutions for the next gap (say, number 4), thus finding 3-gap solutions. We continue adding more gaps until one single k-gap solution stands out in terms of its quality.

The reason why this works is because of what has been described in Section 3: the assumption that there is phase connection for the first gap (in this case number 2) increases the precision of the ephemeris, which is derived from a larger group of connected TOAs. This means that, when we attempt to connect a new gap (in this case 11), the number of acceptable solutions decreases (in this case from three to *two* for each of the two assumptions).

This means that there are acceptable 1-gap solutions for gaps 2 and 11 that do not provide an acceptable solution when they are assumed for both gaps at the same time, i.e. they don't work well together as a 2-gap solution. Since the reduced χ^2 of this 2-gap solution is high, it is unlikely that any k-gap (with $k > 2$) solutions based on this 2-gap solution will have a low reduced χ^2. We can therefore forget about this 2-gap solution when attempting to find the rotation count for the following gaps, i.e. the combination does not pass the χ^2 sieve.

As we will see in Section 5.1 for the specific case of 47 Tuc aa, this sieve is extremely powerful because it decimates the number of possible solutions every time we test the surviving k-gap solutions against gap $k + 1$. The effect might appear to be small at every iteration, but it increases exponentially with every stage. The number of acceptable solutions increases fast at first, but as more gaps are tested, the number of acceptable solutions stabilizes and then starts decreasing. Eventually one solution starts standing out in terms of the quality of the fit. This solution is then generally able to unambiguously connect all other gaps.

4.3 Implementation and future improvements

The relative simplicity of the method outlined above allows a simple implementation as a UNIX shell script (called 'sieve.sh'); this is freely available in the Dracula Github repository,[5] complete with a short description of its usage. The advantage of such a script is that it can run on any UNIX or LINUX platform (which normally have SED and AWK by default), without the need for any special program other than TEMPO.

However, there are still many improvements that could be made to speed up the process and make it more robust.

One improvement that has already been partly implemented is that the script can be made to run much faster by running in shared memory, as in the case of our Github implementation. This avoids writing output files to hard disc, a process that causes disc wear and takes significantly more time than the calculations themselves.

Two further improvements have to do with limitations of TEMPO. The first one is that the values of the reduced χ^2 being reported have a limited range: if they are larger than 999 999.99 they are written by the program as a string of asterisks. In such cases it is impossible to determine the position of the minimum using equation (1). Secondly, each time TEMPO is called it spends most of the time (a) reading clock correction files and correcting the TOAs, (b) reading Earth rotation files and calculating the observatory position, and (c) reading Solar system ephemerides and calculating the Earth position. These operations only need to be done once. We note that the PINT timing program does not have these limitations, and for that reason it will certainly allow much faster discovery of rotation counts.

A fourth improvement has to do with the script itself. In the current version, the user decides which gap is to be connected next. This is not necessarily the gap that yields the smallest number of solutions. An obvious next step is to have the script determine what is the best gap to connect next. This minimization is likely to be very important, since any reduction in the number of solutions at each step has exponential consequences when many steps are considered.

A fifth improvement has to do with an analysis of the timing solutions that are produced with every fit – the information they provide has not been used in the work above. If the estimated positions are well outside the telescope beam, or if the pulsar has a negative $\dot{P}$, then the solutions can be safely excluded. However, the latter condition must be used with care: in a globular cluster, many pulsars have negative $\dot{P}$; as we shall see this is the case for 47 Tuc aa.

Another technique that should provide an extreme acceleration is to parallelize the computation of solutions for successive gaps. This is conceptually very simple: while a version of the script is still searching for solutions for gap A (using the gap mapper), it passes any acceptable 1-gap solutions it finds to a second version of the script working on gap B. This sorts (according to reduced χ^2) the new 1-gap solution against all previous unprocessed 1-gap solutions that have been passed to it from gap A and then works on the best one (deleting it from the list of tasks to do). Assuming that 1-gap solution, it will use the gap mapper to look for solutions for gap B. If it finds any acceptable 2-gap solutions, it will pass them to an analogous script using the gap mapper to find solutions for gap C. This script passes the acceptable 3-gap solutions it finds to an analogous script working on gap D, etc. This saves a lot of time not only because of the parallelism – there is no need to wait for the conclusion of the discovery of all acceptable $(k - 1)$-gap solutions to start searching for k-gap solutions – but also because the sorting by reduced χ^2 at every stage focuses the processing on

[5] https://github.com/pfreire163/Dracula.

Table 3. Successive gaps (order given by k) being tested for 47 Tuc aa; see i numbers in Table 2. Π – product of the n_i for the gaps being tested, which is the number of solutions we would have to test if we were not sieving the acceptable solutions at each stage. N_k – number of k-gap solutions actually being tested at each stage. Here, we can see how this value becomes progressively smaller than Π, demonstrating the power of the sieve technique. In the last column, we indicate the correct solution for these gaps (number 2 of the 30 solutions at step 10). These are small corrections to the rotation count predicted by our initial ephemeris.

k	i	n_i	Π	N_k	Solution
1	2	2	2	2	0
2	11	× 3	= 6	4	1
3	4	× 7	= 42	16	−2
4	14	× 5	= 210	22	−1
5	16	× 13	= 2730	26	6
6	17	× 49	= 133 770	36	31
7	18	× 80	= 107 016 00	90	−33
8	1	× 58	= 620 692 800	135	0
9	3	× 86	= 533 795 808 00	84	−39
10	5	× 115	= 613 865 179 2000	32	25

the best possible solutions first at every stage. This should lead to a bare minimum of TEMPO iterations.

5 TIMING SOLUTION OF 47 TUC AA

Using the technique described in Sections 4.1 and 4.2, we were able to determine a phase-coherent ephemeris for 47 Tuc aa with 1278 TEMPO iterations used in the gap mapper, plus an extra 476 TEMPO iterations that evaluated the quality of valid solutions around minima, plus a similar number of iterations that evaluated non-valid combinations. The first two sets of iterations took a total time of about 3 min. In what follows, we give a detailed account of this process and describe the resulting phase-coherent ephemeris.

5.1 Finding the rotation count for 47 Tuc aa

First, we ran the 'sieve.sh' script looking for solutions for a single gap (gap no. 2 in Table 2), using the gap mapper. There are only two 1-gap solutions, (−1) and (0). Then we ran the same script again to find solutions for gap 11 based on the two 1-gap solutions for gap 2. It found four acceptable 2-gap solutions: (0, 1), (−1, 0), (−1, −1), and (0, 0). Then, for each of these the script searches for acceptable solutions for gap 4, finding 15 acceptable 3-gap solutions. The successive gaps being tested and the number N_k of acceptable k-gap solutions found are listed in Table 3.

The number of k-gap solutions the script has to test at each stage becomes progressively insignificant compared to Π, which is the number of all possible combinations of integers we would have to test if we were not sieving the acceptable solutions at each stage. This number, Π, is the product of the number of 1-gap solutions (n_i) for the gaps already considered. This is a clear demonstration of the power of sieving.

After finding solutions for the tenth gap (number 5 in Table 2), the script starts running into a problem mentioned in Section 4.3: the values of reduced χ^2 at one or more of the sample points used by the gap mapper ($-b$, 0, and b) start becoming too large. This has a good implication: it means that the ephemerides resulting from the assumption of these 10-gap solutions have a strong predictive power, otherwise the values of reduced χ^2 for 'wrong' solutions would not be so large. This is the stage at which we should start looking in more detail at the individual solutions. Fortunately at this stage there are only 32 acceptable 10-gap solutions to look at.

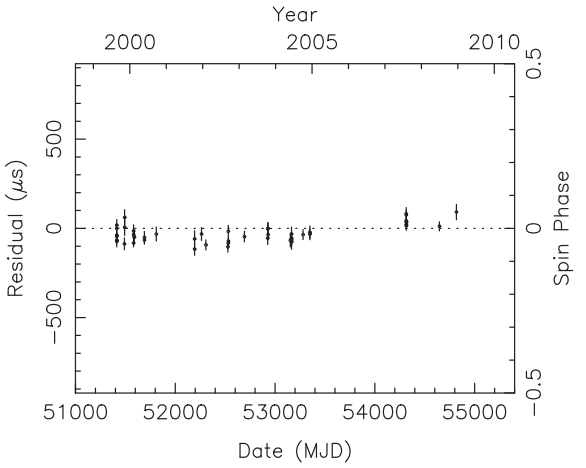

Figure 6. Pre-fit residuals using the ephemeris obtained with the second-best 10-gap solution. The narrow range of phases for all the TOAs outside these 10 gaps indicates that this particular ephemeris is based on the correct rotation count.

We wrote a second script ('test.sh', also found in the Dracula Github repository) that, for any set of k-gap solutions, applies the PHASE statements contained in each of them and then uses TEMPO to derive an ephemeris that assumes that rotation count. Then the script switches to the latter as a starting ephemeris, for this to work it removes all the PHASE statements from the previous TOA list since those are already taken into account by the new ephemeris. If all pre-fit residuals obtained with this ephemeris fall within a relatively narrow phase range, or if they have a clear, slowly varying long-term pattern, then we know we have the correct solution.

Using this script to look at all 10-gap solutions for 47 Tuc aa, we find that the ephemeris based on the second best (reduced $\chi^2 = 1.37$, integers presented in the last column of Table 3) is able to predict all subsequent TOAs to less than 5 per cent of a rotation (see Fig. 6). This behaviour is unique among the 32 acceptable 10-gap solutions. This means that this is the correct solution. Adding these integers to the rotation count predicted by the original ephemeris we obtain the correct rotation count.

We then use the ephemeris derived from the correct 10-gap solution as the new starting ephemeris. This implies we must remove all previous PHASE statements. Furthermore, because we were confident that this ephemeris predicts the correct global rotation count, we can remove all 10 remaining gaps (i.e. we remove all JUMP statements from the remainder of the 'TOA.tim' file) – if we were not yet confident about this, we could use the same sort of test as in Section 3.4 to assure ourselves that we indeed have unique '0' solutions for all remaining gaps. With all gaps removed, we use TEMPO to derive a global phase-coherent ephemeris, with much improved parameters compared to the initial ephemeris. This almost eliminates the small residual trend we still see in Fig. 6, with a post-fit reduced χ^2 that is similar as in the previous step (1.39), despite the fact that 10 degrees of freedom (the JUMP statements) have been eliminated for this fit. This is another strong indication that this is the correct solution. Fitting for μ_α, μ_δ and the second spin frequency derivative ($\ddot{\nu}$), we obtain an even lower reduced χ^2, 1.33. The resulting ephemeris (with the EFAC updated to 1.367 so as to yield a reduced χ^2 of 1.0 and more conservative uncertainty estimates) is presented in Table 4. The parameter uncertainties were derived using a bootstrap method, similar to what is used by Freire

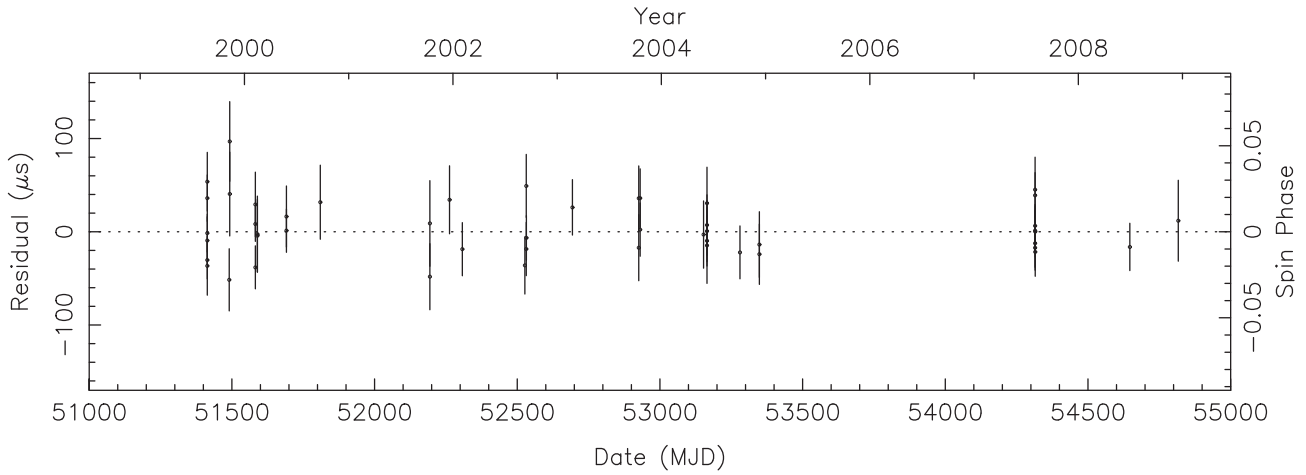

Figure 7. TOA residuals for 47 Tuc aa. Notice the sparseness of the data set. All residuals appear within a narrow range of spin phases, with no JUMP statements needed, furthermore they display no noticeable trends. This is an indication that the ephemeris is correct, i.e. it provides a good description of the observed TOAs and can predict new observations.

Table 4. Timing solution for 47 Tuc aa. The parallax used is derived from the distance to 47 Tuc; it is not fitted.

Observation and data reduction parameters	
Fitting program	TEMPO
Time units	TDB
Solar system ephemeris	DE421
Reference epoch (MJD)	51600
Span of timing data (MJD)	51143–54816
Number of TOAs	49
EFAC	1.367
RMS residual (μs)	26.4
Reduced χ^2	1.00
Timing parameters	
Right ascension, α (J2000)	00:24:07.2783(8)
Declination, δ (J2000)	−72:05:19.5212(35)
Spin frequency, ν (Hz)	541.893 654 948 99(14)
First derivative of ν, $\dot{\nu}$ (10^{-14} Hz s^{-1})	+1.347 54(35)
Second derivative of ν, $\ddot{\nu}$ (10^{-26} Hz s^{-2})	+7.0(2.9)
Proper motion in α, μ_α (mas yr^{-1})	4.6(8)
Proper motion in δ, μ_δ (mas yr^{-1})	−4.6(1.3)
Parallax (mas)	0.2132
Dispersion measure, DM (pc cm^{-3})	24.941(7)
Derived parameters	
Spin period, P (ms)	1.845 380 529 6800(6)
Spin period derivative, $\dot{P}$ (10^{-20} s s^{-1})	−4.5890(15)
Angular offset from centre in α, θ_α (arcmin)	0.123
Angular offset from centre in δ, θ_δ (arcmin)	−0.448
Total angular offset from centre, $\theta_\perp$ (arcmin)	0.465
$\theta_\perp$ (cluster core radii)	1.34
Projected offset from centre, $R_\perp$ (pc)	0.63

et al. (2017). The TOA residuals calculated with this are depicted in Fig. 7. The comparison of some of the parameters with those of the early partial ephemerides is presented in Table 1.

5.2 Timing parameters

The pulsar ephemeris includes a very precise position. As shown in fig. 4 of Freire et al. (2017), the pulsar is located, in projection, almost due South from the centre of the cluster, at a distance of 0.465 arcmin, or 1.34 core radii.

Unlike virtually all pulsars in the Galactic disc, this pulsar (and many others in globular clusters) has a negative $\dot{P}$. For a rotationally powered pulsar, the intrinsic $\dot{P}$ is always positive; this means that, for 47 Tuc aa, this quantity is dominated by the contribution from a negative acceleration of the pulsar in the gravitational field of 47 Tuc (see discussion in Freire et al. 2017). A negative acceleration means that the line-of-sight acceleration of the pulsar is in the direction of the Earth; this implies in turn that the pulsar is in the far half of the cluster. This is expected from the relatively high DM of 47 Tuc aa: previous observations have shown that the pulsars in the far side of the cluster (those with negative $\dot{P}$) have larger DMs than the remaining pulsars. This happens because there is a cloud of ionized gas in the centre of this globular cluster (Freire et al. 2001b). The magnitude of this negative acceleration can be explained by the model of the gravitational field of the cluster presented by Freire et al. (2017), see fig. 6 of that paper.

We also have a marginal detection of $\ddot{\nu}$; this is caused by a change in the line-of-sight acceleration in the gravitational field of the cluster that results from the change of the position of the pulsar in the cluster; these can also be caused by the motion relative to nearby stars. The derived jerk is displayed graphically with the jerks of other pulsars in fig. 7 of Freire et al. (2017).

Since the TOA data set covers a total of 9 yr, we can also measure the proper motion; this is also listed in Table 4. This proper motion is roughly consistent with the proper motion of the remaining pulsars presented by Freire et al. (2017), but it has a lower precision given the small number of TOAs.

The precise location provided by the phase-coherent ephemeris has allowed a detection of the pulsar in X-rays (Bhattacharya et al. 2017), as for the other 22 MSPs in 47 Tuc with such ephemerides. Its X-ray flux is the smallest for any MSP in this cluster. This somewhat surprising find is used to put an upper bound for amplitude of r-mode oscillations in this pulsar as $<2.5 \times 10^{-9}$ and to constrain the shape of the r-mode instability window.

6 CONCLUSIONS

In the first part of this paper we have described a simple technique for determining the correct global rotation count of any pulsar. This technique allows for a simple determination of phase-coherent ephemerides for the vast majority of pulsars. However, for some

pulsars the sparseness and/or low precision of the TOAs does not allow such a simple derivation of the global rotation count.

To solve such cases, we developed an algorithm that tests solutions for k gaps at the same time. Assuming each of the acceptable solutions for $k-1$ gaps, the algorithm searches (using the 'gap mapper') for acceptable solutions for gap number k; if these exist then together with the assumed $(k-1)$-gap solution they make new k-gap solution(s). k is increased until a single k-gap solution becomes clearly superior to the rest. The algorithm naturally eliminates solutions with a bad reduced χ^2 at every step. This is what we call 'sieving'.

This should not be described as a 'brute-force' technique since estimating the suitability of all combinations of acceptable 1-gap solutions would clearly be impractical. Sieving makes the problem not only tractable, but relatively cheap from a computational point of view. Implementing the hierarchical parallel mode described in Section 4.3 and adding automatization should further reduce the amount of time needed to find the correct rotation count with this method; this will likely be necessary for binary pulsars with sparse data sets and/or poor timing precision. We have also suggested changes to TEMPO that would produce further gains in speed and reliability; these issues have already been addressed in the implementation PINT, which will likely be a better vehicle for future development.

We have implemented this technique with a simple shell script, which we have made freely available. We have demonstrated the technique (and its implementation) by finding the correct global rotation count and resultant phase-coherent ephemeris for 47 Tuc aa, an isolated MSP in the globular cluster 47 Tuc with a very sparse set of detections. The scientific implications of the parameters in this ephemeris have already been presented in previous studies.

The automatic determination of the phase-coherent ephemeris for a MSP with such a sparse set of detections implies that this process might be achievable with significantly smaller amounts of telescope time than necessary until now. This will likely become a more pressing issue once high-sensitivity instruments like the SKA come online: this instrument will be finding many thousands of faint pulsars (Keane 2017; Levin et al. 2017) that no other telescope will be able to detect, which means that SKA time for follow-up will be limited for each pulsar.

ACKNOWLEDGEMENTS

We would like to thank our collaborators in the 47 Tuc timing project (Michael Kramer, Dick Manchester, Andrew Lyne, Fernando Camilo, Dunc Lorimer, Christine Jordan, John Sarkissian, and Nichi D'Amico) for collecting and helping to analyse the amazing AFB data set on 47 Tuc over the years. We would also like to thank Norbert Wex and Andrew Cameron for suggestions and comments on the script, and Erik Madsen for his contributions to the Github implementation. Both authors gratefully acknowledge financial support by the European Research Council for the Starting grant BEACON under contract No. 279702, and continued support from the Max Planck Society. Finally, we acknowledge the referee, Dr. Scott Ransom, for valuable suggestions that have significantly improved this work.

REFERENCES

Antoniadis J. et al., 2013, Science, 340, 448
Berti E. et al., 2015, Class. Quantum Gravity, 32, 243001
Bhattacharya S., Heinke C. O., Chugunov A. I., Freire P. C. C., Ridolfi A., Bogdanov S., 2017, MNRAS, 472, 3706
Camilo F., Lorimer D. R., Freire P., Lyne A. G., Manchester R. N., 2000, ApJ, 535, 975
Damour T., Deruelle N., 1986, Ann. Inst. Henri Poincaré Phys. Théor., 44, 263
Damour T., Taylor J. H., 1992, Phys. Rev. D, 45, 1840
Desvignes G. et al., 2016, MNRAS, 458, 3341
Edwards R. T., Hobbs G. B., Manchester R. N., 2006, MNRAS, 372, 1549
Folkner W. M., Williams J. G., Boggs D. H., 2008, Technical Report IOM 343R-08-003, JPL Planetary and Lunar Ephemeris DE421. NASA Jet Propulsion Laboratory
Folkner W. M., Williams J. G., Boggs D. H., Park R. S., Kuchynka P., 2014, Interplanet. Netw. Prog. Rep., 196, 1
Fonseca E. et al., 2016, ApJ, 832, 167
Freire P. C., Kramer M., Lyne A. G., 2001a, MNRAS, 322, 885
Freire P. C., Kramer M., Lyne A. G., Camilo F., Manchester R. N., D'Amico N., 2001b, ApJ, 557, L105
Freire P. C. C. et al., 2017, MNRAS, 471, 857
Hobbs G. B., Edwards R. T., Manchester R. N., 2006, MNRAS, 369, 655
Keane E. F., 2017, preprint (arXiv:1711.01910)
Kopeikin S. M., 1996, ApJ, 467, L93
Levin L. et al., 2017, preprint (arXiv:1712.01008)
Lorimer D. R., 2008, Living Rev. Relativ., 11
Lorimer D. R., Kramer M., 2004, Handbook of Pulsar Astronomy. Cambridge Univ. Press, Cambridge
Özel F., Freire P., 2016, ARA&A, 54, 401
Pan Z., Hobbs G., Li D., Ridolfi A., Wang P., Freire P., 2016, MNRAS, 459, L26
Reardon D. J. et al., 2016, MNRAS, 455, 1751
Ridolfi A. et al., 2016, MNRAS, 462, 2918
Shaifullah G. et al., 2016, MNRAS, 462, 1029
Tauris T. M. et al., 2017, ApJ, 846, 170
The NANOGrav Collaboration, 2015, ApJ, 813, 65
Verbiest J. P. W. et al., 2016, MNRAS, 458, 1267
Wex N., 2014, preprint (arXiv:1402.5594)

SUPPORTING INFORMATION

Supplementary data are available at *MNRAS* online.

Please note: Oxford University Press is not responsible for the content or functionality of any supporting materials supplied by the authors. Any queries (other than missing material) should be directed to the corresponding author for the article.

This paper has been typeset from a TEX/LATEX file prepared by the author.